Nuclear Engineering and Technology 55 (2023) 3401–3408

Contents lists available at ScienceDirect

Nuclear Engineering and Technology

journal homepage: www.elsevier.com/locate/net

Original Article

Monte Carlo simulations for gamma-ray spectroscopy using bismuth nanoparticle-containing plastic scintillators with spectral subtraction

Taeseob Lim [a], Siwon Song [a], Seunghyeon Kim [a], Jae Hyung Park [a], Jinhong Kim [a], Cheol Ho Pyeon [b], Bongsoo Lee [a, *]

[a] School of Energy Systems Engineering, Chung-Ang University, Seoul, 06974, South Korea
[b] Research Center for Safe Nuclear System, Institute for Integrated Radiation and Nuclear Science, Kyoto University, Asashiro-nishi, Kumatori-cho, Sennan-gun, Osaka, 590-0494, Japan

ARTICLE INFO

Article history:
Received 6 April 2023
Received in revised form
18 May 2023
Accepted 22 May 2023
Available online 23 May 2023

Keywords:
Plastic scintillator
Bismuth nanoparticles
Gamma-ray spectroscopy
Monte Carlo N-Particle simulation
Energy resolution

ABSTRACT

In this study, we used the Monte Carlo N-Particle program to simulate the gamma-ray spectra obtained from plastic scintillators holes filled with bismuth nanoparticles. We confirmed that the incorporation of bismuth nanoparticles into a plastic scintillator enhances its performance for gamma-ray spectroscopy using the subtraction method. The subtracted energy spectra obtained from the bismuth-nanoparticle-incorporated and the original plastic scintillator exhibit a distinct energy peak that does not appear in the corresponding original spectra. We varied the diameter and depth of the bismuth-filled holes to determine the optimal hole design for gamma-ray spectroscopy using the subtraction method. We evaluated the energy resolutions of the energy peaks in the gamma-ray spectra to estimate the effects of the bismuth nanoparticles and determine their optimum volume in the plastic scintillator. In addition, we calculated the peak-to-total ratio of the energy spectrum to evaluate the energy measuring limit of the bismuth nanoparticle-containing plastic scintillator using the subtraction method.

1. Introduction

The accurate detection, identification, and quantification of radioisotopes are crucial for national security, particularly for detecting illicit trafficking of radioactive materials at borders. Radiation portal monitoring (RPM) systems are often employed for radioisotope monitoring, and plastic scintillators are commonly used as detectors owing to their ability to detect radiations emanating from large cargo containers [1,2]. Plastic scintillators can be easily manufactured on a large-scale by thermal polymerization of polyvinyl toluene (PVT) or polystyrene (PS) [3,4]. Moreover, they offer several advantages over inorganic scintillators, including faster decay times, nonhygroscopicity, lower manufacturing costs, robustness, easy processability, and good capability for pulse-shape discrimination, which makes them particularly suitable for charged particle detection.

Although plastic scintillators have many advantages, constructing an RPM system solely using plastic scintillators can be challenging. The primary goal of an RPM system is to identify the presence of radiation sources and their nuclides. To identify gamma-ray emitting radioisotopes, gamma-ray spectroscopy using an inorganic scintillator with a multichannel analyzer (MCA) is widely used to distinguish the photoelectric peaks in the corresponding gamma-ray energy spectrum [5,6]. Generally, scintillator materials with high light yields, an excellent light yield proportionality, prompt emission decays, and high effective atomic numbers (Z_{eff}) for high photoelectric cross-sections are required for gamma-ray spectroscopy. However, plastic scintillators have a low Z_{eff} value, and Compton scattering occurs dominantly, resulting in the absence of a full-energy peak in their gamma-ray energy spectra. Notably, the Z_{eff} value of scintillators is crucial to increase the number of photoelectrons generated with energy directly proportional to that of the incident gamma-ray [7–9]. To fulfil this requirement, an RPM system typically uses large-scale plastic scintillators, to detect the presence of radiation sources, and identifies nuclide species using an MCA and inorganic scintillator.

One solution to increase the sensitivity of plastic scintillators for radiation detection is to incorporate constituents with higher atomic numbers, such as bismuth nanoparticles (BNs), while maintaining the benefits of organic scintillators. Bismuth is a

* Corresponding author.
E-mail address: bslee@cau.ac.kr (B. Lee).

https://doi.org/10.1016/j.net.2023.05.030

promising material owing to its high atomic number, low natural radioactivity, low costs, nontoxicity, and low neutron cross-sections. However, incorporating BNs into plastic scintillators can reduce the scintillation yield and make the scintillator turbid, which can affect the emission and absorption wavelengths of the scintillator and increase the self-absorption rate of the scintillating light [10–12]. Bertrand et al. showed that as the weight percentage of bismuth compound increases, the radioluminescence yield and count rate of bismuth-loaded plastic scintillators decrease. Further, bismuth-loaded organic scintillators are sensitive to low-energy gamma nuclides; however, such scintillators are not suitable for RPM systems, which typically require large-area measurements [13–16].

In this study, we developed a new method for drilling holes on the surface of plastic scintillators and filling them with BNs to achieve the same effect as that of bismuth-loaded plastic scintillators. Incident gamma-rays interact with these bismuth-filled holes, resulting in the production of photoelectrons that produce photoelectric peaks in the gamma-ray energy spectrum. Moreover, the transparency and self-absorption rate of the plastic scintillator, containing evenly drilled holes filled with BNs, remain almost unaffected, unlike the properties of bismuth-loaded plastic scintillators, and these drilled plastic scintillators can be easily produced in large sizes. However, because the density of BNs in these scintillators is higher than that of the bismuth dopants in bismuth-loaded plastic scintillators, larger holes may shield gamma-rays. Therefore, optimizing the amount of BNs in plastic scintillators is critical to ensure a highly efficient gamma-ray spectroscopy. Additionally, we used the Monte Carlo N-Particle (MCNP) simulation program to evaluate the performance of BNs in the plastic scintillator. The photoelectric peak in the energy spectrum obtained from the BN-containing plastic scintillator (BNPS) was identified by subtracting the energy spectrum from that of the original plastic scintillator (OPS) without BNs. The full width at half maximum (FWHM) and energy resolutions of the photoelectric peaks were calculated to evaluate the performance of the proposed BNPS.

2. Materials and methods

Prior to performing the simulation, it is necessary to consider the Gaussian energy broadening (GEB) effect, which produces a Gaussian distribution of energies for monoenergetic particles. The desired FWHM is specified as follows [17]:

$$FWHM = a + b\sqrt{E + cE^2} \quad (1)$$

where E is the energy of the gamma-ray source in MeV; and a, b, and c are user-provided constants (UPCs), which were determined through experiments conducted using gamma-ray emitting radionuclides. UPCs are essential input data of MCNP simulation for obtaining energy spectra, and we selected gamma-ray sources such as ^{57}Co (E_{peak} = 122.06 keV and 136.47 keV), ^{137}Cs (E_{peak} = 661.72 keV), and ^{60}Co (E_{peak} = 1117 keV and 1332 keV) whose activities are 3.92, 8.36 and 9.42 μCi, respectively. Normally, the main gamma-ray emitting target sources of RPM include ^{133}Ba, ^{57}Co, ^{137}Cs, and ^{60}Co [18]. In our experiments, we use three gamma-ray emitting radionuclides considering the wide range of their peak energies, which range from 122.06 to 1332 keV.

Fig. 1 shows the experimental setup used to determine the GEB constants. A cylindrical plastic scintillator (50 mm in diameter and 30 mm in height, Epic crystal) was employed to convert the energy of the incident particles into visible light signals, which were then amplified by a photomultiplier tube (PMT, R6233-100, Hamamatsu photonics). Additionally, a charge sensitive preamplifier (2005, Mirion Technologies) was used to amplify the height of the pulse output obtained from the PMT. Finally, a digitizer (DT5725, CAEN) was used to receive and classify the signals according to their energy.

Fig. 2 shows the gamma-ray energy spectra of ^{57}Co, ^{137}Cs, and ^{60}Co, which are measured using a PVT plastic scintillator to decide the Compton maxima (CM) of each gamma-ray emitting radionuclide. There are no full energy peaks or Compton edges in the spectrum of the incident gamma-rays due to the low density of a PVT. Normally, CM can be found at the end of Compton continuum of the plastic scintillator, which is located at the lower energy region compared with the position of Compton edge. The linear relationship between the CM energy and the energy of the Compton edge enables the former to be used for the energy calibration of plastic scintillators. Specifically, the energy of the CM in energy spectra is related to the base material and size of the scintillators [19–21]. In this study, we calculated the CM of a cylindrical plastic scintillator made of PVT with a diameter of 5 cm and a depth of 3 cm, using the method described by Lukasz Swiderski et al. [19]. ^{137}Cs is a monoenergetic source that produces a single photopeak, whereas the spectra of ^{57}Co and ^{60}Co show two photoelectric peaks that combine form a CM as shown in Fig. 2. Therefore, we used the deconvolution method to analyze the CM accurately. Fig. 2 shows the deconvoluted CM energy peaks of each gamma-ray source as dotted lines. For each peak, the CM energy was fixed and the deconvolution process was performed using Origin software (OriginPro 2021, OriginLab). For ^{137}Cs, and ^{60}Co, the CM energies were clearly shown as peaks. However, the CM peak for ^{57}Co was not clearly visible in the measured spectrum due to the low density of the plastic scintillator. The CM energy for ^{57}Co was determined based on the discontinuous point observed on the spectrum.

Table 1 shows the energy and FWHM of the CM of each gamma-ray source. To extract the optimum values of the UPCs, the FWHM of the CM are substituted into Equation (1), and an iterative calculation method is employed [22]. The obtained values of a, b, and c are 0.0414, 0,0566, and 0.6254, respectively, and the corresponding graph is depicted in Fig. 3.

Fig. 4 shows the composition of BNPS used in MCNP simulation. The plastic scintillator included 19 cylindrical holes filled with BNs to evenly distribute BNs, with a center-to-center distance of 9.6 mm. BNs were represented as nanoscale particles by dividing bismuth-contained holes into voxels with a width, height, and depth of 100 nm each. The gamma-ray source was located 5 cm away from the center of the scintillator surface and emitted in 2π direction, and the standard gamma-ray energies of the sources were 100, 300, 500, 700, 900, and 1100 keV. The types of BNPSs were categorized based on the diameter and depth of the holes, which were adjusted between 1 to 5 mm and 5–25 mm, respectively, while considering the size of the original scintillator. Consequently, the total volume of the BNs in the plastic scintillator was varied from 74.58 to 9321.88 mm^3. Further, the BNPSs were divided into 20 types to increase the volume of the BNs linearly. Finally, the gamma-ray energy spectra for each energy were simulated using the BNPSs and OPS. Table 2 shows the detailed composition types of BNPS simulated to find the optimal design.

The subtraction method was applied to evaluate the effect of the BNs on the gamma-ray detection performance. Fig. 5(a) shows the simulated 500-keV gamma-ray energy spectra of the OPS and BNPS (contains 19 holes, each with a diameter of 2 mm and depth of 25 mm). Photoelectric peaks are absent in both the energy spectra of the OPS and BNPS, but noticeable differences appear in the incident gamma-ray energy region, such as at ~500 keV, as shown in Fig. 5(a). The number of counts corresponding to the peak at ~500 keV is higher for BNPS than for OPS. However, a distinct energy peak is obtained by subtracting the energy spectrum of OPS from that of BNPS as shown in Fig. 5(b). The FWHM and energy

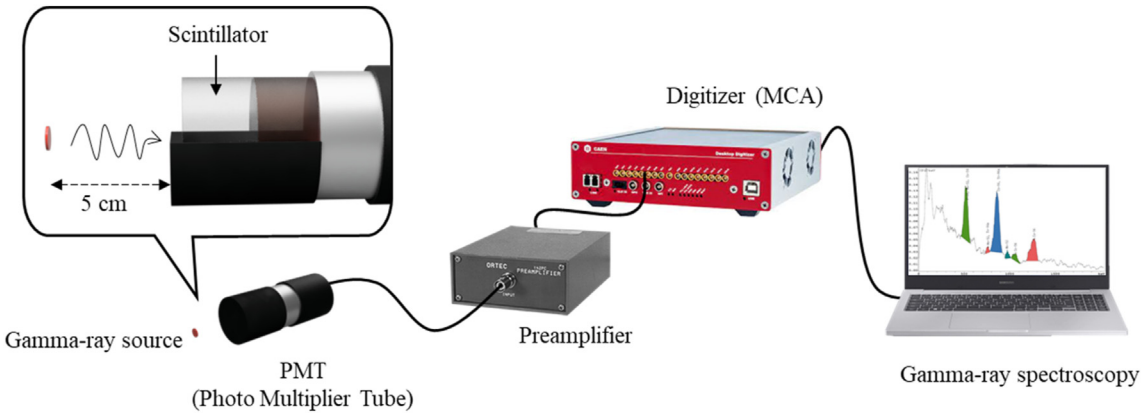

Fig. 1. Experimental setup for measuring CM to determine the GEB constants.

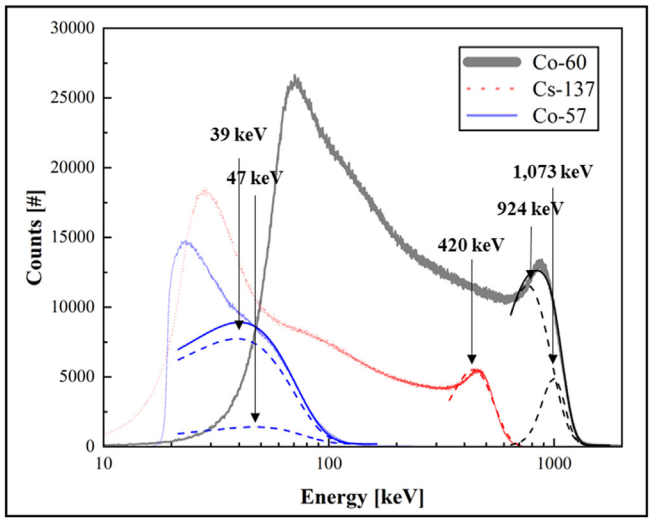

Fig. 2. Gamma-ray energy spectra of ^{57}Co, ^{137}Cs, and ^{60}Co.

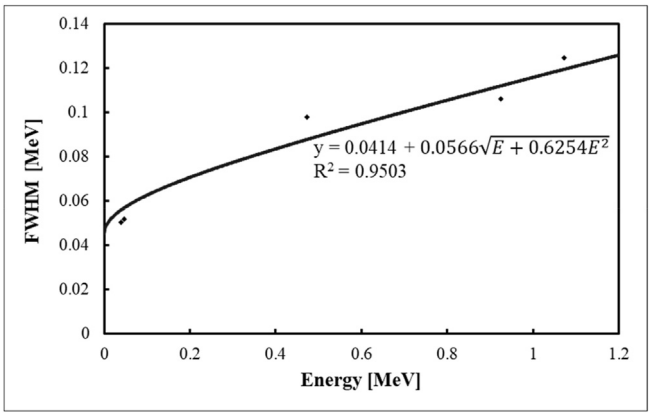

Fig. 3. Relationship between FWHM and gamma-ray energy to determine the optimal UPCs for analyzing the GEB effect.

Table 1
Energies and FWHM of the CM.

Gamma-ray source	Energy of CM [MeV]	FWHM [MeV]
^{57}Co	0.03946	0.0506
	0.04751	0.0519
^{137}Cs	0.42064	0.0981
^{60}Co	0.92485	0.1062
	1.08446	0.1248

resolution of the peak in the subtracted energy spectrum, whose profile varies with the volume of the BNs in the plastic scintillator and are calculated to estimate the gamma-ray detection performance of the BNPS. The optimum design of the BNPS is also determined by adjusting the diameters and depths of the bismuth holes. In this study, all the MCNP simulations were repeated 10^8 times to reduce relative errors to below 1%, and the activity of the gamma-ray source was set to 10 μCi.

3. Experimental results

The gamma-ray spectra, with energies from 100 to 1100 keV, detected by the OPS were used as the references in the spectral subtraction method. The MCNP simulated gamma-ray spectra of energies 100, 300, 500, 700, 900, and 1100 keV detected by the OPS are shown in Fig. 6(a). The y-axis of the energy spectra is adjusted to a logarithmic scale to identify the energy peaks efficiently. Evidently, no photoelectric peak appears in all these energy spectra. Fig. 6(b) presents the gamma-ray energy spectra of the BNPS, which has BN-containing holes (diameter: 2 mm; depth: 25 mm), irradiated by various gamma-ray energy sources. Similar to the results of the OPS, no significant peak is observed in the energy spectra of the BNPS. Notably, the counts collected within the incident gamma-ray energy range is noticeably different for the two scintillators. However, the subtracted spectra displayed in Fig. 6(c) show distinct gamma-ray peaks.

As mentioned above, the gamma-ray detection performance of the BNPS can be evaluated by varying the volume of the BNs, i.e., by adjusting the diameters and depths of the BN-containing holes. To evaluate the effect of the hole diameter, the depth of the holes was fixed at 15 mm, while the diameters were varied from 1 to 5 mm. To compare the subtracted energy spectra obtained at various energy ranges, gamma-ray energies of 100 to 1100 keV were used in the MCNP simulations. Fig. 7 shows Gaussian curves fitted to the subtracted energy spectra obtained at different gamma-ray energies by varying the hole diameter and fixing the hole depth. As the gamma-ray energy decreases, the peaks in the subtracted spectra shift to lower energies because of the high stopping power of the BNs, and this tendency fades as the energy levels increase. The energy resolution and heights of the peaks in the subtracted energy spectra vary depending on the incident gamma-ray energy. However, the

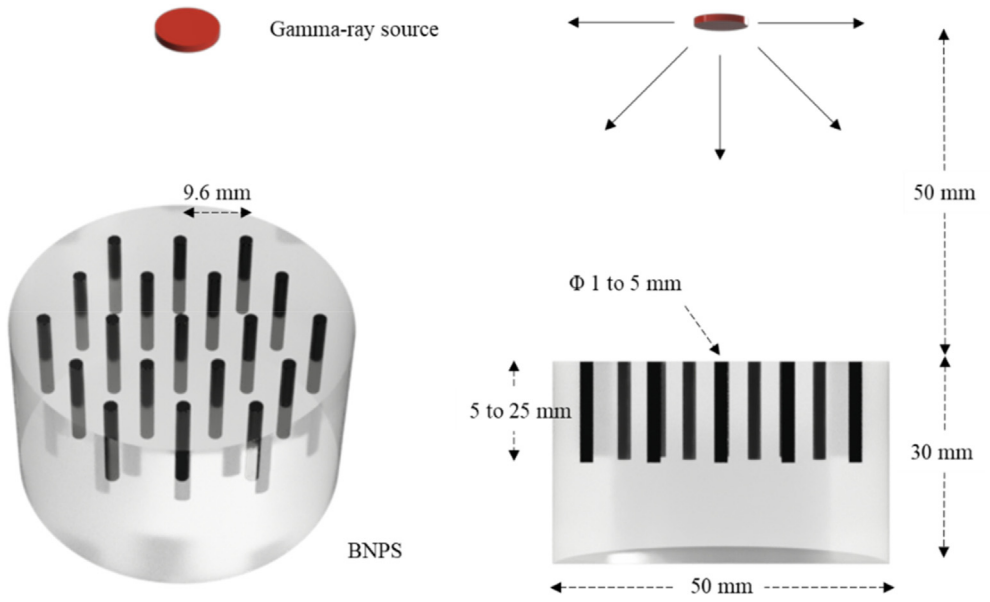

Fig. 4. Composition of the BNPS used in the MCNP simulation.

Table 2
Composition types of BNPS simulated to find the optimal design.

Type	Diameter [mm]	Depth [mm]	Volume [mm^3]	Type	Diameter [mm]	Depth [mm]	Volume [mm^3]
1	1	5	74.58	11	3	20	2684.70
2	1	15	223.73	12	3	25	3355.88
3	1.6	20	763.65	13	4	15	3579.60
4	1.6	25	954.56	14	4	27	6443.28
5	2	5	298.30	15	4	20	4772.80
6	2	15	894.90	16	4	25	5966.00
7	2	20	1193.20	17	5	15	5593.13
8	2	25	1491.50	18	5	18	6711.75
9	3	15	2013.53	19	5	20	7457.50
10	3	18	2416.23	20	5	25	9321.88

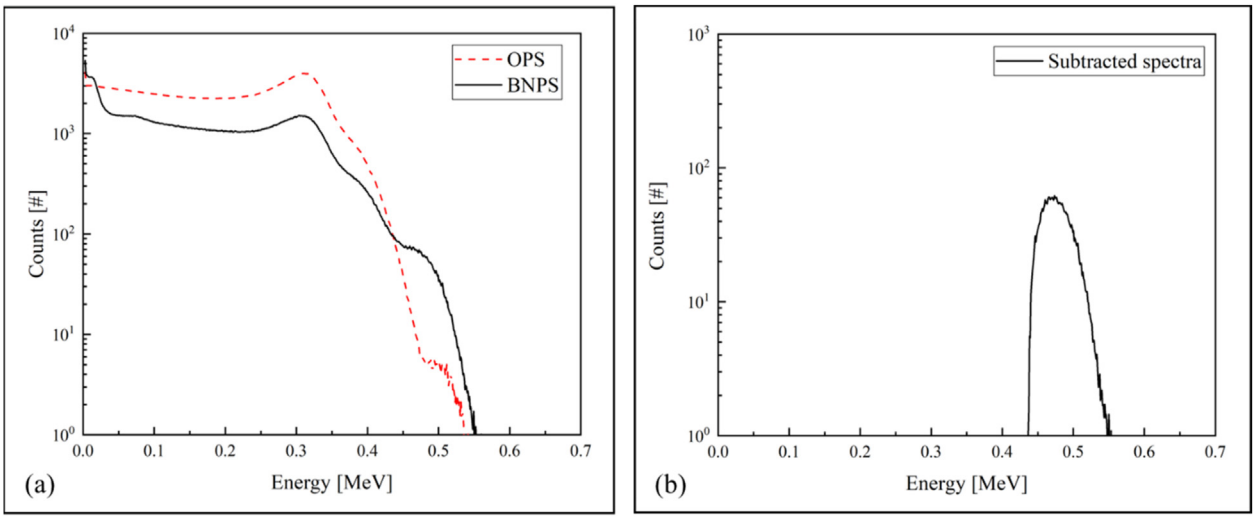

Fig. 5. (a) Simulated energy spectra of a 500-keV gamma-ray source irradiated on the OPS and BNPS, and (b) the distinct energy peak obtained by subtracting the energy spectrum of OPS from that of BNPS.

best performance is achieved in all the cases when the hole diameter is 2 mm. Our simulation results suggest that the optimal hole diameter should be 2 mm for the BN-containing holes in this study. To measure and evaluate the FWHM and energy resolution efficiently, the energy peaks were fitted with a Gaussian fitting model using Origin. The fitting was iterated until the coefficient of determination (R^2) exceeded 0.9 for each result.

Conversely, the subtracted spectra with a fixed diameter of

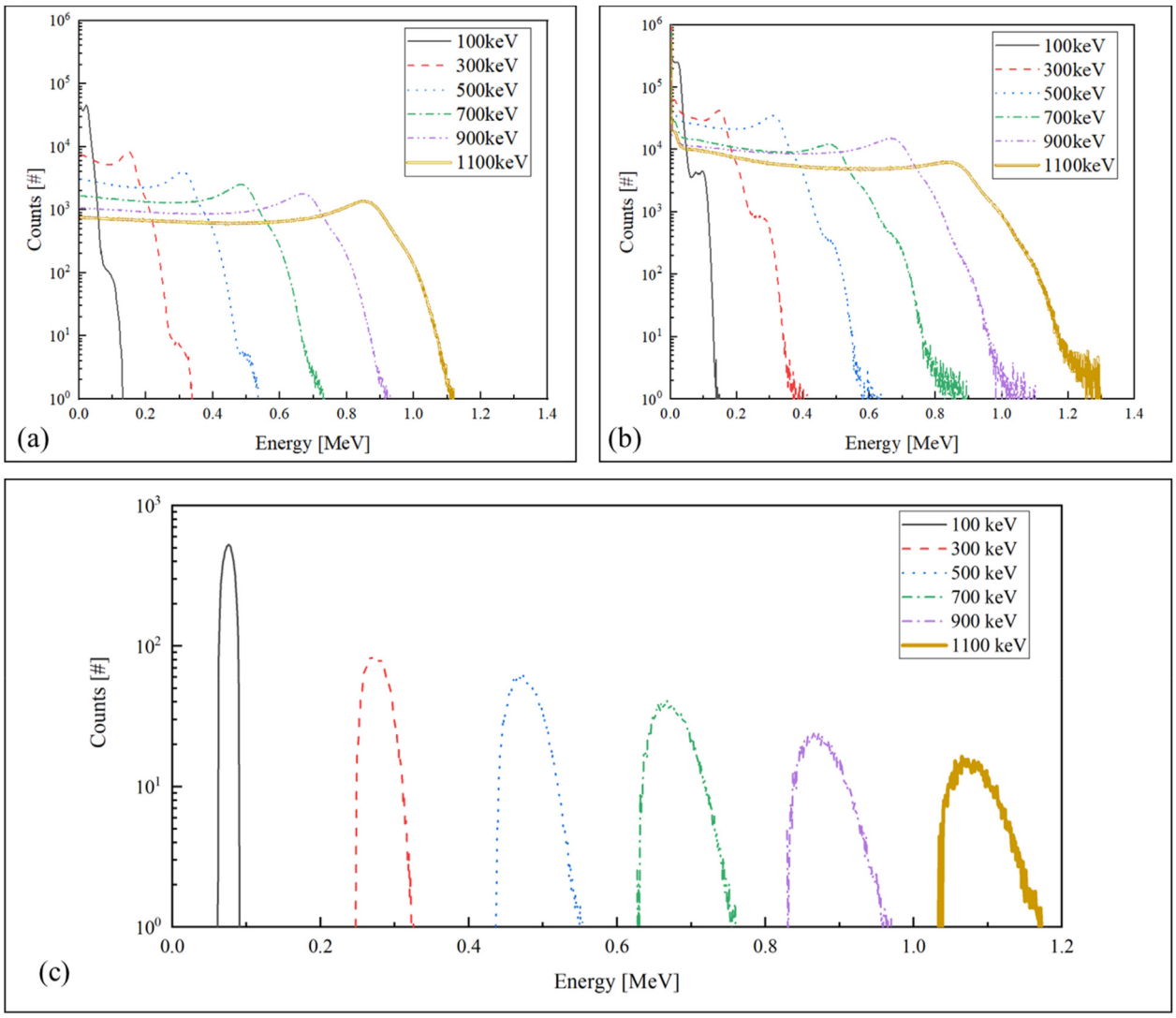

Fig. 6. MCNP simulated gamma-ray energy spectra of the (a) OPS and (b) BNPS, and (c) the energy peaks determined using the subtraction method.

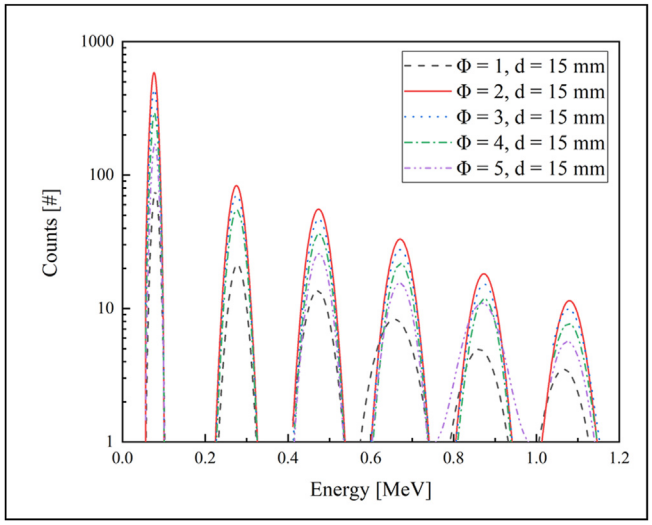

Fig. 7. Gaussian curves fitted to the subtracted energy spectra obtained at different gamma-ray energies (100, 300, 500, 700, 900, and 1100 keV) by fixing the hole depth to 15 mm.

2 mm were analyzed by varying the depth of the holes. BNPSs with depths of 5, 15, and 25 mm were used to evaluate the correlation between the hole depth and energy resolution of the energy peaks. Similar to the previous case, Gaussian curve fitting was employed to analyze the peak attributes as depicted in Fig. 8. Evidently, in all the gamma-ray energy regions, the energy peak becomes narrower with the increasing hole depth. This observation indicates that the FWHM decreases, and the resulting energy resolution improves with the increasing hole depth. These results collectively demonstrate that a BNPS with 25-mm-deep holes exhibits the best gamma-ray detection performance. According to the results of Figure 7 and 8, the optimal design for BN-containing hole in PVT cylindrical scintillator used in this study was determined to be 2 mm in diameter and 25 mm in depth.

The performance of the BNPS is ultimately affected by the volume proportion of the BNs present in the scintillator. If the size of the scintillator is changed, then the amount of BNs must also be adjusted accordingly. Fig. 9(a) shows the energy resolutions of the subtracted spectra at different volume ratios of the BNs in the scintillator. Evidently, the energy resolutions, at all the gamma-ray energies, enhance as the volume percentage of the BNs increases from 0% to 2.5. However, the slope of the graph becomes less steep

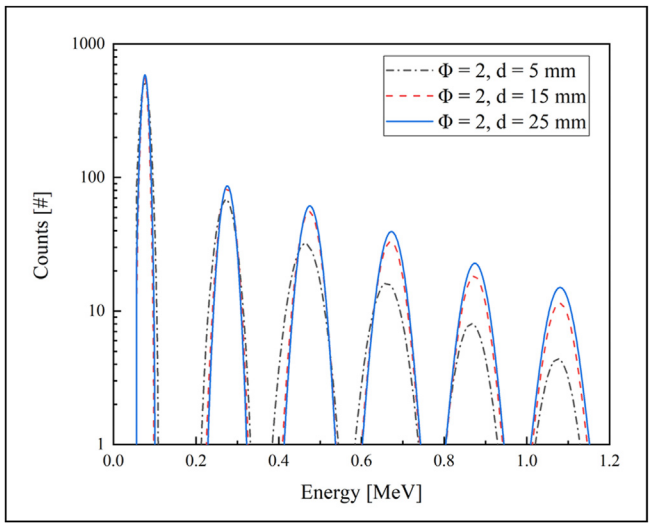

Fig. 8. Gaussian curves fitted to the subtracted energy spectra obtained at different gamma-ray energies (100, 300, 500, 700, 900, and 1100 keV) by fixing the hole diameter to 2 mm.

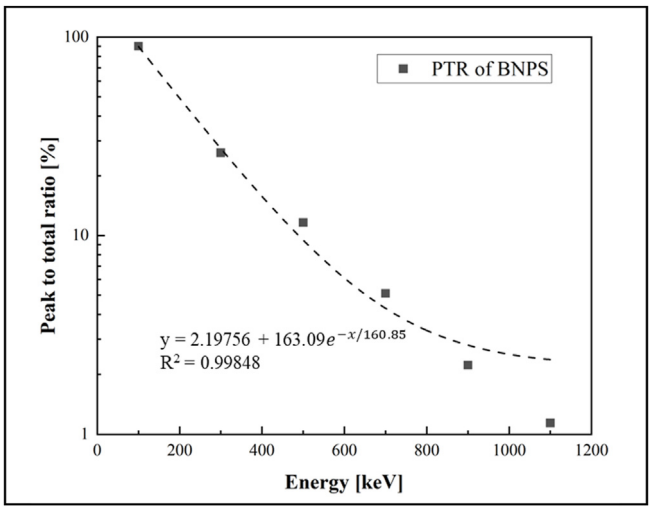

Fig. 10. PTR of the subtracted spectra detected using the optimally designed BNPS.

as the amount of bismuth contained in the scintillator increases. The energy resolution sharply enhances until the total volume of the BNPS occupied by the BNs reaches approximately 2% as indicated in Fig. 9(b), which shows the resolution enhancement trend observed between 0% and 3% volume ratios.

The gamma-ray energy detection limit of the BNPS and subtraction method can be determined by calculating the peak-to-total ratio (PTR), which indicates the correlation between the area under the photoelectric peak and the total area within the spectrum. The PTR can be determined using the following formula [23,24]:

$$PTR = \frac{Area\ under\ the\ photopeak}{Total\ area\ in\ the\ spectrum} \quad (2)$$

The PTR of the subtracted spectra for each gamma-ray energy is calculated using the simulation values obtained from the optimally designed BNPS, which has 19 holes (2 mm in diameter, 25 mm in depth) that cover 2.53% of the total scintillator volume as demonstrated in Fig. 10. A low PTR indicates that long-time data acquisition is required to obtain a statistically significant number of counts under the photopeak. As the energy of gamma-rays increases, the PTR exponentially decreases. In this study, PTR >10% for the subtracted energy peaks was considered practical. Up to ~500 keV (intermediate energy range), we obtained PTR >10%, whereas at higher energies, the PTR value significantly decreased to below 10%. Thus, the identification of higher energy peaks would require a significant amount of time.

Finally, we compared the photopeak detection performance of the BNPS with spectral subtraction with that of the bismuth-loaded plastic scintillator demonstrated by Cherepy et al. [11]. In their study, a bismuth-loaded plastic scintillator, with a volume of 231.4 cm^3 (10.4 cm × 8.9 cm × 2.5 cm) and loaded with 20 wt% of bismuth tripivalate, was used to detect the photopeak of ^{241}Am, ^{57}Co, and ^{137}Cs gamma-ray sources. Fig. 11 shows the Gaussian curve fitted energy peaks of ^{241}Am, ^{57}Co, and ^{137}Cs. The simulation was conducted using the optimally designed BNPS, and the photon counts were converted into an arbitrary unit using the maximum values of each source before the Gaussian fitting.

Table 3 lists the energy resolutions of the gamma-ray energies

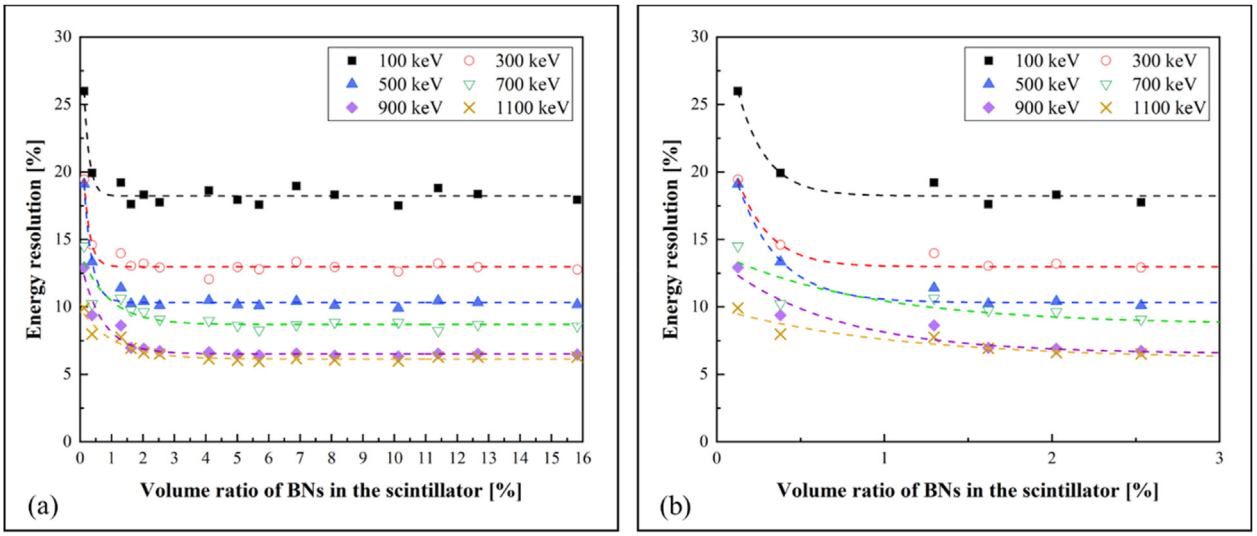

Fig. 9. (a) Energy resolutions of the photopeaks in all the subtracted spectra, and (b) resolution enhancement trend observed between 0% and 3% volume ratios.

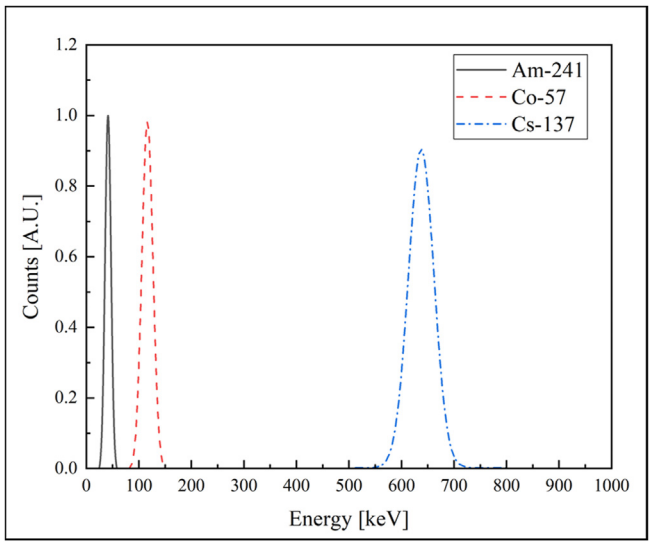

Fig. 11. Subtracted energy peaks of ^{241}Am, ^{57}Co, and ^{137}Cs with Gaussian fitting.

Table 3
Energy resolution of the BNPS (with MCNP simulation) and a bismuth-loaded plastic scintillator (Cherepy et al. [11]) at the standard energies emitted by the gamma-ray sources.

Gamma-ray sources	Energy resolution [%]	
	BNPS	Bismuth-loaded plastic scintillator
^{241}Am (59 keV)	22.51	49
^{57}Co (122 keV)	16.27	28
^{137}Cs (662 keV)	8.61	16

emitted by the three radioactive sources and detected by the BNPS (deduced via MCNP simulations) and bismuth-loaded plastic scintillator reported by Cherepy et al. [11]. Evidently, the energy resolution of the BNPS using the subtraction method is more enhanced than that of the previously reported bismuth-loaded plastic scintillator at all the standard energies emitted by these three gamma-ray sources (^{241}Am, ^{57}Co, and ^{137}Cs).

4. Conclusions

In this study, we simulated the gamma-ray spectra measured by an OPS and BNPS using the MCNP program. The BNPSs were designed by drilling holes on the surface of a plastic scintillator and filling them with BNs. For the BNPSs, the counts in the energy spectrum at any incident gamma-ray energy were higher than those detected by the OPS. To generate the energy peak that was absent in the original spectra of both the scintillators, we subtracted the BNPS and OPS spectra. The FWHM (i.e., criterion for performance evaluation) of the peak in the subtracted spectra varied with the volume percentage of the BNs in the BNPS. We adjusted the diameter and depth of the holes to vary the proportion of the BNs and determined the optimum design for detecting gamma-rays from radioisotopes. The results demonstrated that the BNPS with 19 BN-containing holes (diameter: 2 mm; depth: 25 mm) showed the best performance. The changes in the energy resolution could not be distinguished when the volume proportion of the BNs was over 2.5% of the total volume of the BNPS. The observed changes in the energy resolution gradient due to the increased BN volume indicated that the BNPS showed the best gamma-ray detection performance in the intermediate energy range around 500 keV. Furthermore, we confirmed the gamma-ray energy detection limit of the optimum BNPS and subtraction method be calculating the PTRs of the detected energy spectra. Evidently, this optimally designed BNPS can efficiently detect gamma-ray photons in the intermediate energy range of ~500 keV, whereas at energies above 700 keV, the photopeak detection efficiency of the BNPS drastically degrades. Additionally, we compared the gamma-ray detection performance of the designed BNPS, based on the subtraction method, with that of a previously reported bismuth-loaded plastic scintillator using three different gamma-ray sources, namely ^{241}Am, ^{57}Co, and ^{137}Cs. We observed that at all the photopeak energies, the resolution of the BNPS surpassed that of the bismuth-loaded plastic scintillator. In the future, based on these simulation results, a BNPS-based detector will be manufactured, and gamma-ray detection performance will be experimentally investigated using radionuclides and the subtraction method presented in this paper.

Declaration of competing interest

The authors declare that they have no known competing financial interests or personal relationships that could have appeared to influence the work reported in this paper.

Acknowledgements

This research was supported by the National Research Foundation of Korea (NRF) grant funded by the Korean Government (MSIT) (No. 2020M2D2A2062457, 2022M2D4A1084440) and the Korea Institute of Energy Technology Evaluation and Planning (KETEP) grant funded by the Korean Government (MOTIE) (No. 20201520300060).

References

[1] J. Ely, R. Kouzes, et al., The use of energy windowing to discriminate snm from norm in radiation portal monitors, Nucl. Instrum. Methods Phys. Res. Sect. A Accel. Spectrom. Detect. Assoc. Equip. 560 (2) (2006) 373–387.
[2] H.C. Lee, B.T. Koo, et al., Evaluation of source identification method based on energy-weighting level with portal monitoring system using plastic scintillator, J. Rad. Protect. Res. 45 (3) (2020) 117–129.
[3] S. Min, H. Kang, et al., Integrated and portable probe based on functional plastic scintillator for detection of radioactive cesium, Appl. Sci. 11 (11) (2021) 5210.
[4] D. Yu, P. Wang, et al., Two-dimensional halide perovskite as beta-ray scintillator for nuclear radiation monitoring, Nat. Commun. 11 (1) (2020) 3395.
[5] G.F. Knoll, Radiation Detection and Measurement, John Wiley & Sons, 2010.
[6] K. Kovler, S. Levinson, et al., Scintillation vs. Semiconductor Spectrometers for Determination of Norm in Building Materials, 2014.
[7] E.R. Siciliano, J.H. Ely, et al., Comparison of pvt and nai(tl) scintillators for vehicle portal monitor applications, Nucl. Instrum. Methods Phys. Res. Sect. A Accel. Spectrom. Detect. Assoc. Equip. 550 (3) (2005) 647–674.
[8] Z. Cho, C. Tsai, L. Eriksson, Tin and lead loaded plastic scintillators for low energy gamma-ray detection with particular application to high rate detection, IEEE Trans. Nucl. Sci. 22 (1) (1975) 72–80.
[9] N. Cherepy, H. Martinez, et al., New plastic scintillators for gamma spectroscopy, neutron detection and imaging, in: 2017 IEEE Nuclear Science Symposium and Medical Imaging Conference (NSS/MIC), IEEE, 2017, pp. 1–3.
[10] B.L. Rupert, N.J. Cherepy, et al., Bismuth-loaded Polymer Scintillators for Gamma Ray Spectroscopy, MRS Online Proceedings Library (OPL), 2011, p. 1341.
[11] N.J. Cherepy, S. Hok, et al., Bismuth-loaded plastic scintillator portal monitors, in: Hard X-Ray, Gamma-Ray, and Neutron Detector Physics XX, vol. 10762, SPIE, 2018, pp. 10–15.
[12] T.J. Hajagos, C. Liu, et al., High-z sensitized plastic scintillators: a review, Adv. Mater. 30 (27) (2018), e1706956.
[13] G.H.V. Bertrand, F. Sguerra, et al., Influence of bismuth loading in polystyrene-based plastic scintillators for low energy gamma spectroscopy, J. Mater. Chem. C 2 (35) (2014).
[14] S. O'Neal, N. Cherepy, et al., Performance of high stopping power bismuth-loaded plastic scintillators for radiation portal monitors, IEEE Trans. Nucl. Sci. 67 (4) (2020) 746–751.
[15] M. Hamel, F. Carrel, Pseudo-gamma spectrometry in plastic scintillators, in: New Insights on Gamma Rays, 2017 ch. (Chapter 3).
[16] G.H.V. Bertrand, J. Dumazert, et al., Understanding the behaviour of different

metals in loaded scintillators: discrepancy between gadolinium and bismuth, J. Mater. Chem. C 3 (23) (2015) 6006–6011.
[17] W. Metwally, R. Gardner, A. Sood, Gaussian broadening of mcnp pulse height spectra, Trans. Am. Nucl. Soc. 91 (2004) 789–790.
[18] Andrei Stavrov, Eugene Yamamoto, Real breakthrough in detection of radioactive sources by portal monitors with plastic detectors and New Advanced Source Identification Algorithm (ASIA-New), in: International Conference on Advancements in Nuclear Instrumentation Measurement Methods and Their Applications, ANIMMA, 2015, p. 4, 2015.
[19] L. Swiderski, M. Moszyński, et al., Measurement of compton edge position in low-z scintillators, Radiat. Meas. 45 (3–6) (2010) 605–607.
[20] E.R. Siciliano, J.H. Ely, et al., Energy calibration of gamma spectra in plastic scintillators using compton kinematics, Nucl. Instrum. Methods Phys. Res. Sect. A Accel. Spectrom. Detect. Assoc. Equip. 594 (2) (2008) 232–243.
[21] B. Stríbrnský, M. Petriska, R. Hinca, Energy calibration of plastic scintillator detector, in: Presented at the Applied Physics of Condensed Matter (Apcom 2019), 2019.
[22] C. Kim, Y. Kim, et al., Iterative Monte Carlo simulation with the compton kinematics-based geb in a plastic scintillation detector, Nucl. Instrum. Methods Phys. Res. Sect. A Accel. Spectrom. Detect. Assoc. Equip. 795 (2015) 298–304.
[23] H. Leutz, G. Schulz, L. Van Gelderen, Peak/total-ratios for NaI(Tl)-crystals, Nucl. Instrum. Methods 40 (2) (1966) 257–260.
[24] P. Limkitjaroenporn, W. Hongtong, et al., PTR, PCR, and energy resolution study of gagg: Ce scintillator, in: Journal of Physics: Conference Series, vol. 970, IOP Publishing, 2018, 012016, 1.